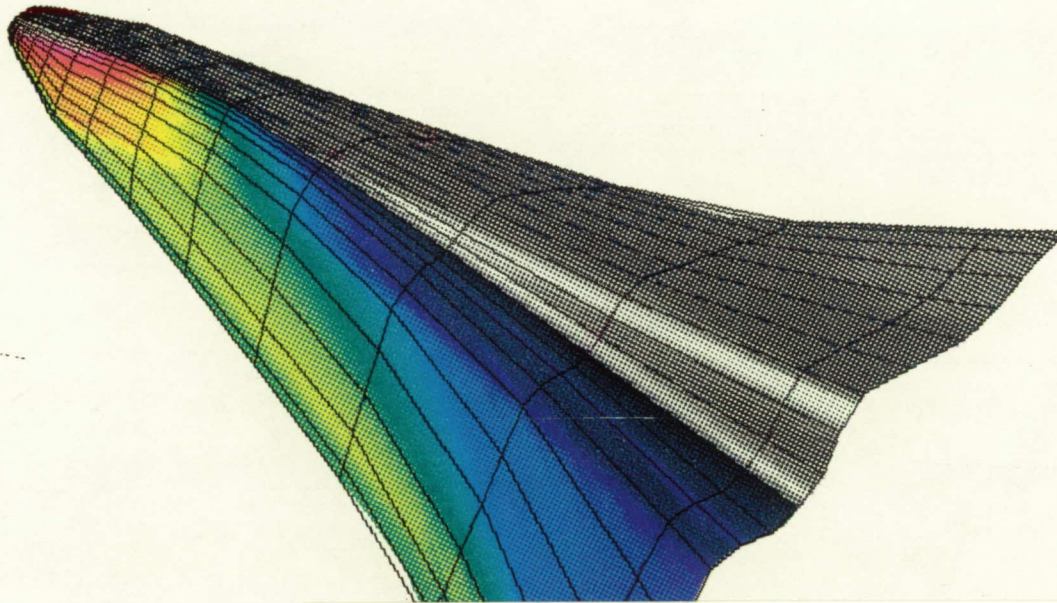


493780 ~~82867~~
IN-05-CR
145805
P.13

HSCT Mission Analysis of Waverider Designs
NASA Langley Award NAG-1-1295, Acct. 153-6442



(NASA-CR-192193) HSCT MISSION
ANALYSIS OF WAVERIDER DESIGNS
Quarterly Progress Report No. 2, 15
Aug. 1991 - 15 Nov. 1992 (Colorado
Univ.) 13 p

N93-21646

Unclas

G3/05 0145805

Summary of 2nd Quarter Contract Work
(August 15, 1991 - November 15, 1992)

ORIGINAL CONTAINS
COLOR ILLUSTRATIONS

Nomenclature

| | |
|------------|--|
| AR | = aspect ratio |
| C_D | = drag coefficient, $D/(q_\infty S_{ref})$ |
| C_L | = lift coefficient, $L/(q_\infty S_{ref})$ |
| C_M | = moment coefficient, $M/(q_\infty S_{ref} L_{ref})$ |
| C_V | = volume coefficient V/L_{ref}^3 |
| D | = drag |
| L | = lift |
| L/D | = lift over drag |
| M | = moment about the configuration's nose |
| L_{ref} | = reference length (symmetry plane chord length) |
| q_∞ | = freestream dynamic pressure |
| Re | = Reynolds number based on L_{ref} |
| S_{ref} | = reference area (planform area) |
| S_{wet} | = wetted area |
| X_{ac} | = streamwise aerodynamic center |
| X_{cent} | = streamwise centroid |
| V | = volume |
| ξ | = axial curvilinear coordinate |
| η | = circumferential curvilinear coordinate |
| ζ | = radial curvilinear coordinate |
| η_v | = volumetric efficiency ($V^{2/3}/S_{wet}$) |

Summary of Previous Contract Work

Work in the first project quarter was primarily directed toward the development of two waverider design algorithms. WIPAR, the interactive waverider design code, was developed to the point that confident inviscid calculations of the lower surface flow properties could be made and assessed. The ability to perform real-time manipulation of the functions that control surface geometry allowed for the rapid creation of high lift-to-drag waverider configurations. More importantly, however, the interactive nature of the software allowed the user to create true waveriders that were much more practical-looking than the waveriders of previous studies; a big step in the direction of configurations that are realistic candidates for a Mach 4 High-Speed Civil Transport mission. In addition, the algorithm of SCIEMAP (Supersonic Cross-stream Inverse Euler Marching Program) was outlined, and fundamental analytic work was carried out supporting the method and defining the approach's strengths, weaknesses, and limitations.

Second Quarter Progress

In the second quarter the development of the two waverider design tools was continued, and the groundwork necessary for the incorporation of waverider technology into the realm of the HSCT's was laid out. Advances in each of these areas is summarized below.)

WIPAR

Work on the WIPAR code included the addition of an upper surface geometry generator and characteristic flow solver and the inclusion of viscous analysis in the performance computations. Details of these changes are given below.

Upper Surface Generation Waverider upper surfaces in most previous studies have been freestream surfaces (aligned with the direction of the freestream velocity). In our case, however, it is desirable to geometrically refine the upper surface for two reasons. First, we want to eliminate, if possible, the existence of a blunt base. Blunt bases are notoriously difficult to analyse computationally because of strong pressure gradients at the truncation that tend to produce an unpredictable flowfield. There are empirical formulas to deal with this problem, but disagreement between methods abounds. From a design and performance standpoint it is much more reasonable to close the configuration at the exit plane in such a way that the upper surface pulls gently toward the lower surface and closes at the effective trailing edge of the aircraft. Control of the upper surface governing functions is applied in such a way that the thickness at each location within the planform projection (a function of streamwise and spanwise coordinate) can be slightly deviated from the upper surface that exists for the freestream case. The constraints are that these deviations must be smooth, the surface must close at the exit plane (as described above), and any ramp-type upper surface feature that generates a compression region must be a small angular perturbation. The pressure on the upper surface is calculated by means of a local axisymmetric method of characteristics approximation. Local surface normal lines are determined and used as the marching domain for the method. A fourth-order Runge-Kutta scheme determines pressure and Mach number of the next downstream point based on information from the last point and the local surface geometry. Once data for all points in the marching lines has been determined, the values are redistributed to the original grid. Comparison of the surface pressure determined in WIPAR with F3D flow solver computations shows excellent agreement, indicating that for reasonable upper surface geometries, the method is quite robust.

Figure 1 shows a comparison between surface pressure values obtained directly from the interactive program WIPAR and results from the proven flow solver, F3D. The right side of the configuration (as viewed) is the upper surface pressure distribution generated interactively in WIPAR. The left side of the configuration is colormapped to pressure values obtained from F3D. The adjacent graph shows the magnitude of upper surface

pressure values at approximately 50% span as a function of streamwise location on the configuration. There are actually two graphs, one for the WIPAR data and one for the F3D data but the results are in such good agreement that the discrepancy is not apparent at the scale shown. It is important to point out at this time that the results obtained in WIPAR took approximately .2 seconds to compute on a Silicon Graphics IRIS 4D35 GT Workstation, while the F3D results required over 15 minutes of CPU time on the NASA Langley CRAY YMP to generate.

Viscous Analysis Viscous effects play a large role in the performance of vehicles in these hypersonic flight regimes. Therefore, a rigorous viscous analysis should be applied to accurately track the development of the viscous boundary layer and include its subsequent contributions to performance. A significant achievement of the second quarter's work has been the implementation of viscous analysis in WIPAR. Observed L/D values for an inviscid computation are misleading because they neglect the heavy drag penalty that results from boundary-layer interactions. This is quite evident in the overall configuration L/D, which typically drops 30-40% when viscous effects are included.

To perform the analysis in WIPAR the method of White and Cristoph¹ is implemented, which has produced results in excellent agreement with experimental data over the laminar, transitional, and turbulent flow regimes in previous studies. As in the method of characteristics analysis discussed above, surface normal marching lines are determined from the surface geometry on both the upper and lower surfaces. Using the surface pressure and Mach number at each successive streamwise station the local skin-friction coefficient is determined. The values are interpolated onto the computational mesh and are used, along with the inviscidly determined surface pressure values, to calculate the configuration performance.

Observation of the viscous penalties when using WIPAR interactively is particularly interesting, because it underscores the importance of designing configurations whose volume to wetted surface area ratio is high. As a measure of this quality a nondimensional parameter, the volumetric efficiency (η_v), is defined as the ratio of the volume to the two-thirds over the wetted area. Some previous studies have defined η_v with respect to the planform area instead of the wetted area. Logically this is a poor choice as it would be possible for a vehicle with an infinite surface area and a finite volume to have a nonzero volumetric efficiency. Improving volumetric efficiency typically involves localizing the internal volume to the centerline and thinning the "wing-like" features.

With these design concerns in mind, several promising candidates have been generated in WIPAR for the Mach 4 HSCT mission scenario. The first configuration has essentially a full length delta planform with a rectangular cross-section fuselage and a blunted nose. This case shall be referred to as HSCT1 in the following text. The second case, denoted HSCT2, is a sharp-nosed configuration with a compound planform wing sweep. This sweep concentrates more lifting surface at the rear of the aircraft, effectively shifting the aerodynamic center rearward. If the forward section of both these aircraft can accommodate

enough high-density cargo to place the C.G. at a sufficiently upstream position, the configurations should prove statically stable. Tabulated below are geometric and performance parameters for each of the two configurations. An optimized Mach 4 waverider due to Bowcutt et al.² is also included in the table for purposes of comparison. The configuration surface geometries associated with these results are graphically illustrated in figs. 2, 3, and 4.

Table 1: WIPAR performance results.

| | HSCT1 | HSCT2 | Bowcutt Mach 4 |
|------------|-------|-------|----------------|
| C_L | 0.070 | 0.085 | 0.091 |
| C_D | 0.012 | 0.016 | 0.016 |
| L/D | 6.04 | 5.32 | 5.84 |
| C_M | 0.049 | 0.057 | 0.060 |
| C_V | 0.009 | 0.010 | 0.010 |
| S_{ref} | 0.427 | 0.356 | 0.490 |
| η_v | 0.046 | 0.055 | 0.052 |
| AR | 0.780 | 0.761 | 0.829 |
| X_{ac} | 0.713 | 0.699 | 0.680 |
| X_{cent} | 0.668 | 0.675 | 0.636 |

SCIEMAP

The SCIEMAP routine, like WIPAR, is proposed for the design of waverider forebodies. However, where WIPAR is restricted to shock waves of constant strength (homotropic flow), SCIEMAP is not. As with virtually all waverider design methods, SCIEMAP first defines the flowfield behind a prescribed shock surface and then carves the waverider's lower surface from the flowfield as an inviscid streamsurface. Most previous waverider design studies have limited the choice of shock shapes to very simple geometric surfaces such as planes, cones, or perhaps even general axisymmetric surfaces. WIPAR extends the selection to include virtually any constant strength shock surface, but SCIEMAP makes no restrictions except that the shock must be physically possible, that is, it may have no slope discontinuities and the local shock angle must remain between the Mach angle and the weak shock limit.

In the course of the second project quarter much of the analysis performed during

the first quarter has been incorporated into a working computer code. To date, utilities have been developed for the definition of arbitrary 3-D shock surfaces, the computation of post-shock flow conditions, and the marching of the solution in a roughly cross-stream direction away from the shock surface. These utilities are briefly described in the following sections.

Shock Definition The shape of the shock surface that is to be generated by the resulting waverider configuration must be specified as input. Ideally the surface should be defined parametrically such that the partial derivatives on the surface are known analytically. In its current form many simple geometries such as a plane or a cone can be generated as well as very general shapes with curvature in both the streamwise and cross-stream directions as illustrated in fig. 5a. The computational mesh on the shock surface is formed using an integration technique designed to maximize the stability of the marching procedure.

Post-Shock Conditions The post-shock flow conditions are the actual initial conditions for the marching procedure, and hence, the accuracy of the marched solution depends on the accuracy of their computation. They can be quite easily defined using the Rankine-Hugoniot shock jump relations and some straight-forward vector algebra. The post-shock pressure on the shock surface of fig. 5a. with a freestream Mach number of 4 and a specific heat ratio of 1.4 is shown in fig. 5b. Note that the pressure is not constant illustrating the varying shock strength. Note also that the flow will not be homentropic, but it will still be isentropic, that is, the entropy may not be constant everywhere, but it will be constant along a particle path.

Marching Procedure The development of the marching procedure involved the bulk of the work effort on SCIEMAP. This is primarily due to the inherent ill-posedness of the problem. Using a much simpler linearized model equation to represent the coupled set of 3-D, nonlinear, hyperbolic partial differential equations that govern the flows of this study, it can easily be shown that marching outside of the characteristic conoids results in an unstable algorithm that diverges exponentially. However, it can also be shown that a similar 2-D problem is well-posed, that is marching can be done stably in any direction except along characteristics. By marching in a direction that eliminates the cross-flow velocity and minimizes cross-derivatives, the effects of the problem's ill-posedness can be suppressed, and a physically meaningful solution can be obtained.

The equations used to govern the flow are the conservation of mass, momentum, and entropy. The choice of the entropy equation rather than the more commonly used energy equation is valid for inviscid, adiabatic flows, and it weakens the coupling between the five equations reducing the computational effort required for their solution. The equations are nondimensionalized and transformed into a generalized curvilinear coordinate system. The gradients in one computational direction (normal to the shock surface) are solved for in terms of gradients in the other two computational directions which are already known

on the shock surface. The solution can then be integrated away from the shock. The computational grid must be generated in a step by step fashion as its geometry is solution dependent. The marched grid and solution for the example shock surface are shown in fig. 5c. Pressure isofringes at several grid cross-sections, on the symmetry plane, and on the last marched grid plane are shown. Note the solution may not be marched outside of the characteristic domain defined by the given shock surface, hence, the back boundary of the computational domain must be reduced at each marching step as shown.

Configuration Analysis

During the second quarter groundwork for the analysis of complete configurations was initiated. This involved the development of computational utilities for the integration of powerplants with the waverider forebodies, and the acquisition of a number of configuration analysis software packages. Work in these areas is discussed in the following sections.

Powerplant Integration A large part of this project involves successfully integrating a powerplant on the waverider configuration. The engine to be used is a hypothetical afterburning turbojet that has been incorporated into a previous NASA Langley developed Mach 4 HSCT concept due to Domack et al.³. Aside from some minor geometric considerations, engine placement and fairing geometry is really quite arbitrary. For the purpose of making the integration sufficiently simple that a rapid on-design analysis can be made, the engine fairing will be assumed to have sidewalls that lie within a region of local osculation in the lower surface flowfield. The engine inlet lip shape is defined as an arbitrary curve whose enclosed area satisfies the inlet mass flow requirement. The lower surface is then defined by streamlines emanating from the inlet lip and traced in the streamwise direction to the exit plane of the configuration. In following this design procedure, the pressure values on all facets of the fairing are well-known and can then be applied, along with the inlet and nozzle conditions to determine the full engine contribution to the aircraft performance. Examples of these integrated engine fairings can be seen in figs. 2, 3, and 4.

Configuration Analysis Software Four configuration analysis software packages were obtained from NASA Langley. These include the AEROS code for aerodynamic analysis in the subsonic range, LAR-13223 for the determination of zero-lift wave-drag, Gentry's code for the evolution of arbitrary hypersonic bodies, and the FLOPS code for mission evaluation and optimization. Use of the software for analysis of complete configurations was held up due to a delay in the delivery of the relevant documentation and user manuals, however, installation of the packages on local workstations was successfully accomplished, and their application should be quickly forthcoming.

Summary

The new results obtained over the course of the last quarter of research are encouraging. Revolutionary waverider geometries have been generated that could potentially be worthy candidates for a Mach 4 regime high-speed civil transport mission. All modules are in place for a comprehensive point-design analysis of generalized non-conical waverider configurations. The next quarter's work will seek to choose several promising HSCT candidates and explore their off-design performance characteristics, especially within the low-speed regime. Major component packaging will also be checked, to insure that these configurations can indeed accommodate the fuel, passengers, and avionics necessary to successfully complete the selected mission.

References

- ¹ White, F. M., Viscous Fluid Flow, McGraw-Hill, New York, 1974, pp. 653-657.
- ² Bowcutt, K. G. Anderson, J. D., and Capriotti, D., "Viscous Optimised Hypersonic Waveriders," AIAA Paper No. 87-0272, Jan., 1987.
- ³ Domack, C. S., Dollyhigh, S. M., Beissner, F. L. Jr., Geiselhart, K. A., McGraw, M. E. Jr., Shields, E. W., and Swanson, E. E., "Concept Development of a Mach 4 High-Speed Civil Transport," NASA TM 4223, Dec. 1990.

Comparison of WIPAR and F3D Data

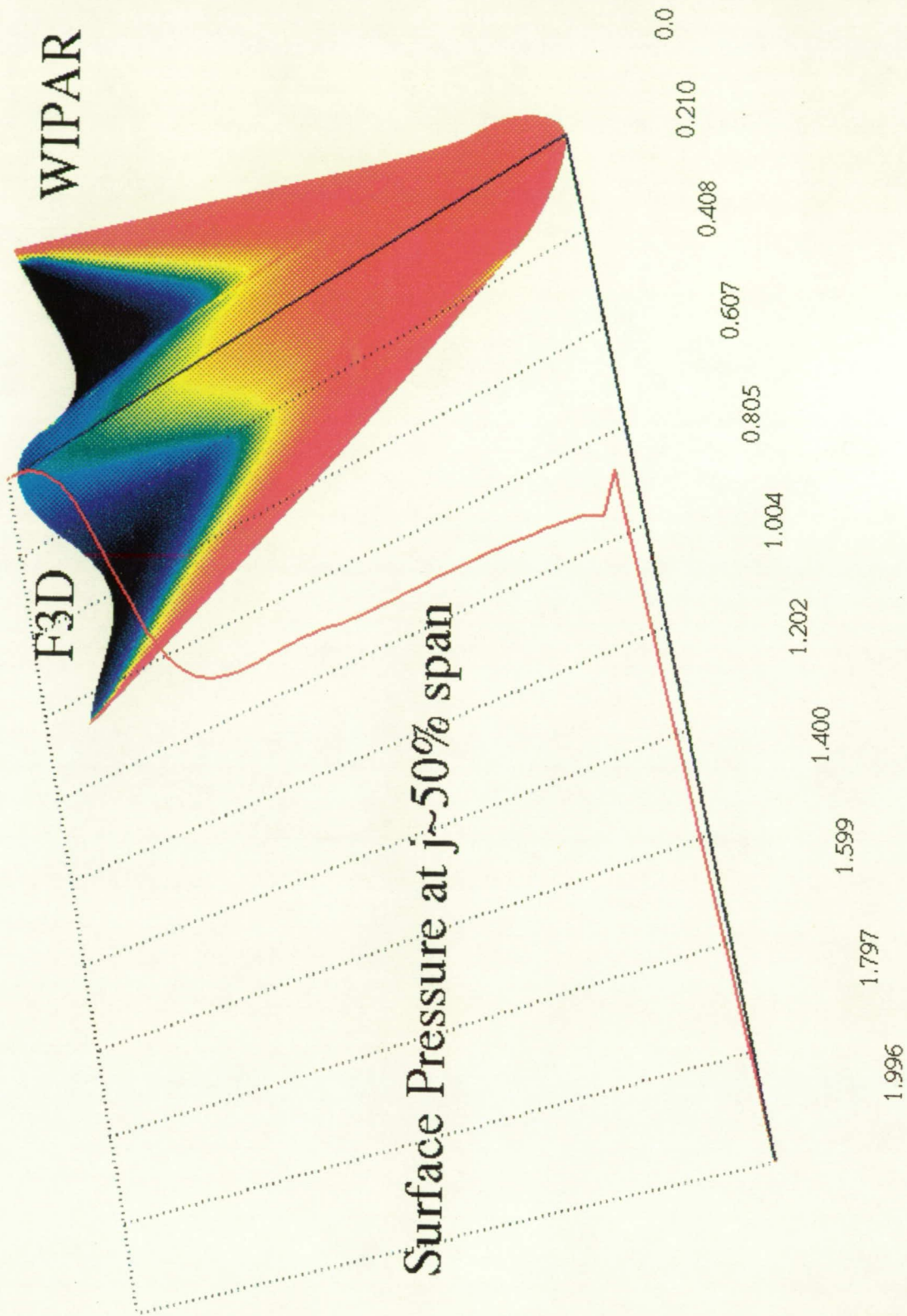


Figure 1: Comparison of WIPAR surface pressures and surface pressures obtained using the F3D flow solver. Graph on the left contrasts the surface pressure values of each set of data at approximately 50% span.

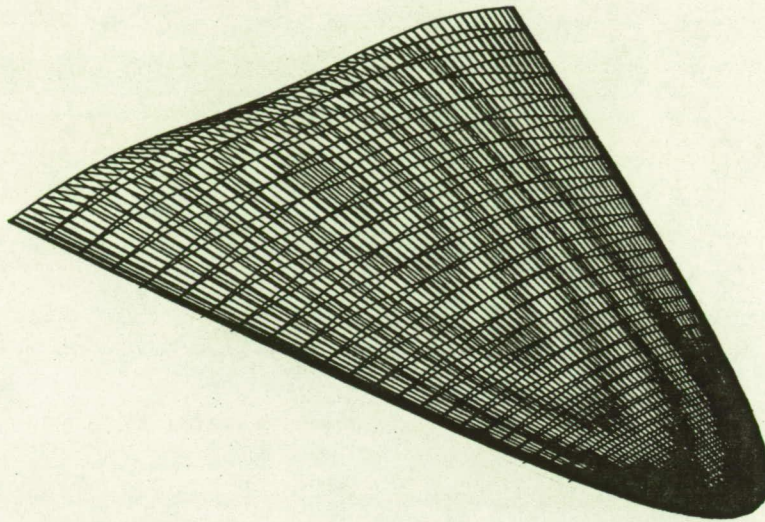


Figure 2a: Perspective view of Bowcutt's optimum Mach 4 waverider with a closed exit plane.

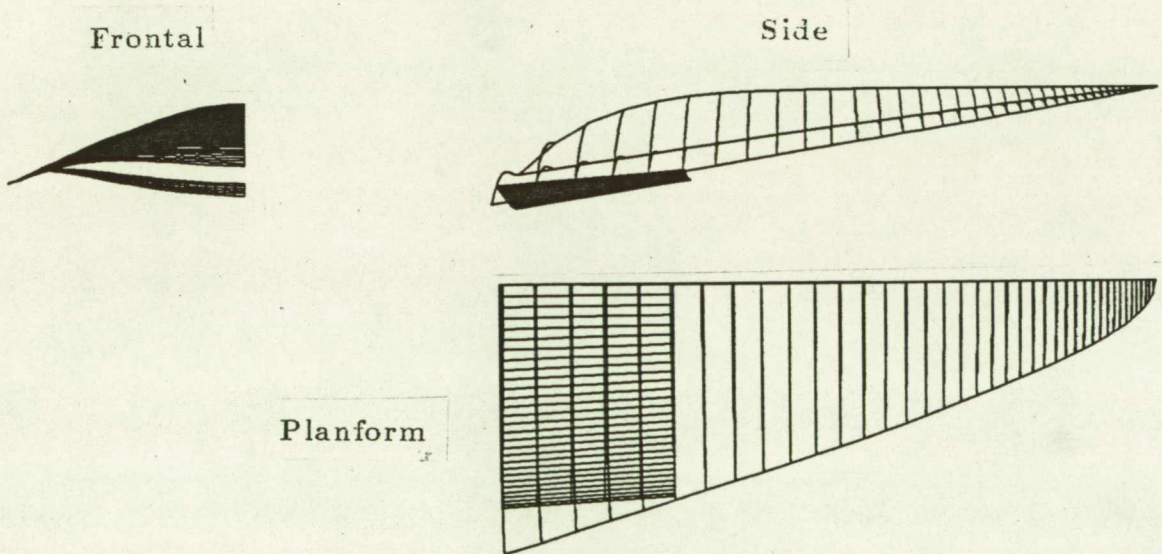


Figure 2b,c,d: Frontal, side, and planform views of the Bowcutt configuration.

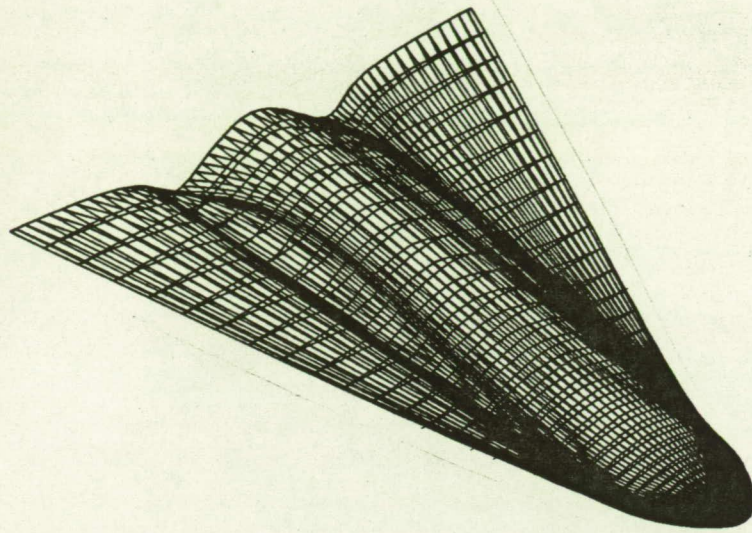


Figure 3a: Perspective view of configuration HSCT1.

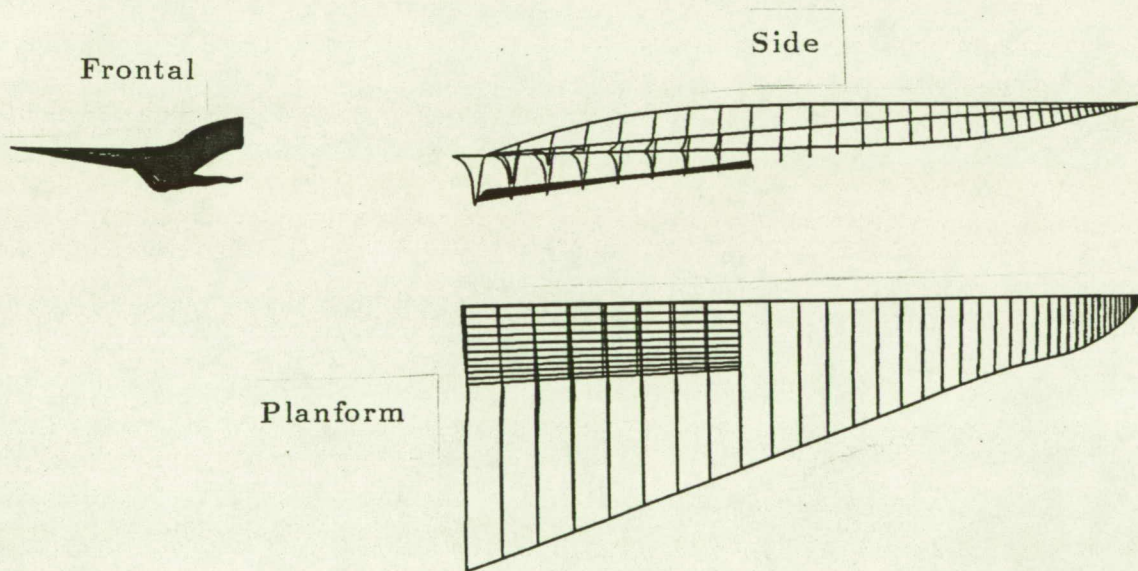


Figure 3b,c,d: Frontal, side, and planform views of the HSCT1 configuration.

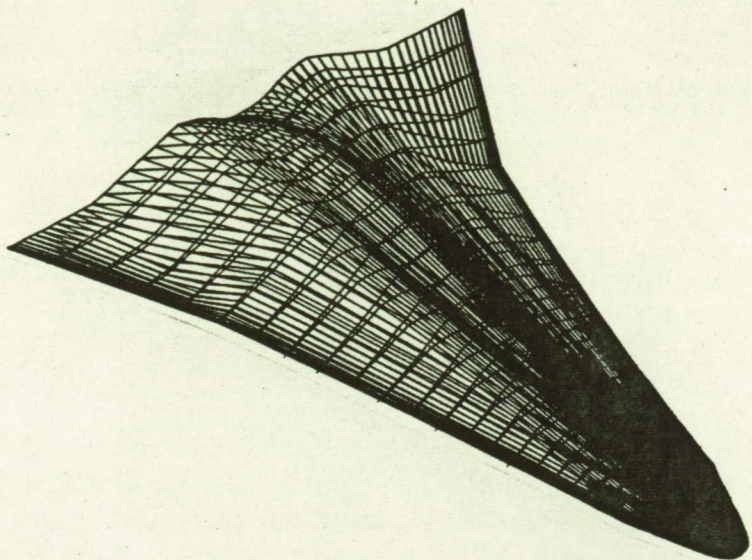


Figure 4a: Perspective view of configuration HSCT2.

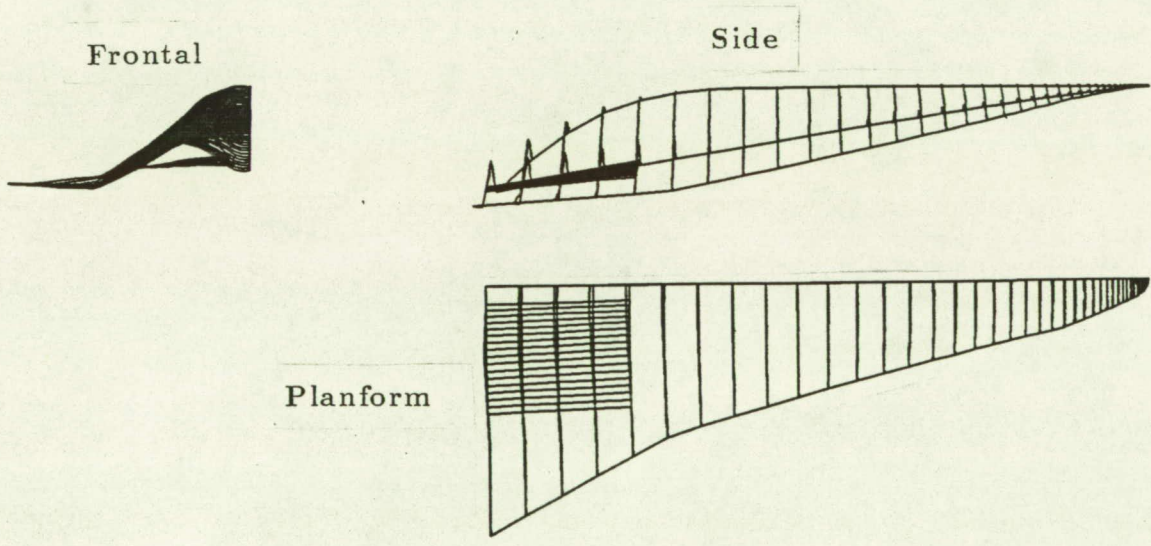


Figure 4b,c,d: Frontal, side, and planform views of the HSCT2 configuration.

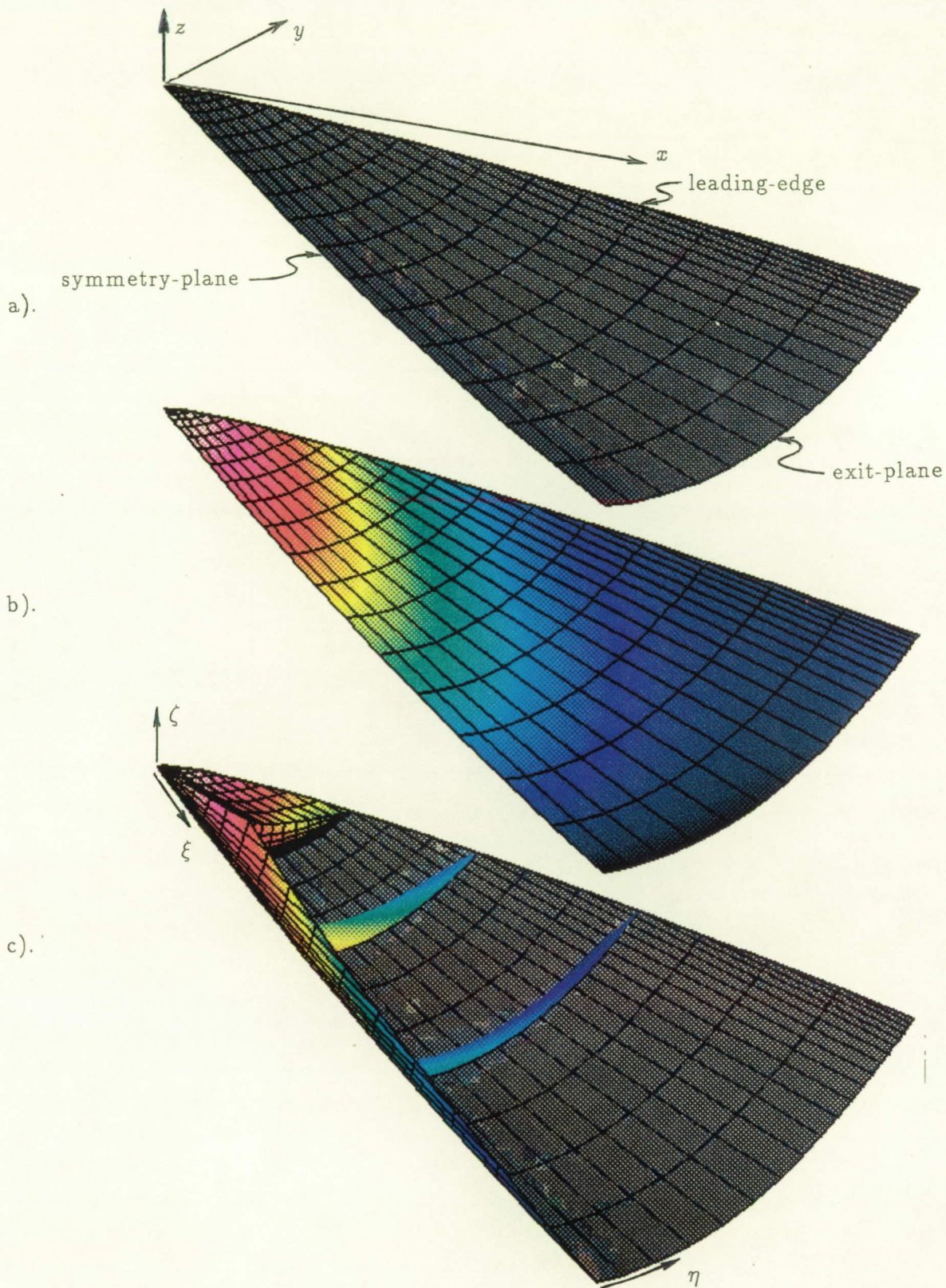


Figure 5: SCIEMAP results; a). shock surface with initial mesh, b). post-shock pressure distribution, and c). marched grid and pressure distributions.